PAPER

Two-Dimensional Arrays Optimized for Wide-Scanning Phased Array Based on Potential Function Method

Koji NISHIMURA[†a)] *and* **Toru SATO**[††], *Members*

SUMMARY For phased and adaptive arrays of antennas, an optimal arrangement of antenna elements is essential to avoid grating lobes in the visible angular region of the array. Large sidelobes cause degradation in signal-to-noise ratio; grating lobes, in the worst case, cause malfunctions. One method of evaluating sidelobe level is square integration. For a given set element positions, evaluation by square integration of the sidelobes involves Fourier transform and numerical integration. For faster evaluation, we developed an equivalent transform algorithm that requires no numerical Fourier transform or integration. Using this new algorithm, we introduced a fast trial-and-error algorithm that iteratively applies random perturbation to the array, evaluates the function, and minimizes it. A number of separate runs of this algorithm have been conducted under the constraint of 3-fold rotational symmetry for stability. The optimal output, for which the function is minimized, is a uniformly spaced equilateral-triangular-type arrays that, unfortunately, has unwanted grating lobes. However the algorithm also yields variations trapped at local minima, some of which do not have grating lobes and whose sidelobe peaks are sufficiently low within a wide angular region. For the case $N = 12$, a characteristic triagular-rectangular-type array often arises, which has not only better sidelobe properties as evaluated by square-integration and peak sidelobe, but also sufficient element-to-element clearance. For the case $N = 36$, one of the results achieves a peak-sidelobe level of -8 dB, with a minimum element-to-element separation of 0.76 wavelength.

key words: *two-dimensional array optimization, adaptive array, sidelobe reduction*

1. Introduction

Antenna array are used for various purposes, such as to selectively retrieve significant radio signals from background interference, and to concentrate transmission energy in a certain direction. In any such scenario, the spatial response is an essential component of an antenna array. Large sidelobes within the angular region of interest can make selective retrieval difficult. Grating lobes–a special case of sidelobes–can cause selective retrieval to fail altogether between these directions and the mainlobe. Sidelobes or grating lobes can also cause signal energy to leak. It is therefore important that undesired sidelobes, including grating lobes that arise in a uniform array, should be reduced to avoid such degradations.

In adaptive array applications, where the excitation of each antenna element is controllable, sidelobes can be suppressed to a certain extent by adjusting the excitation of the elements. However, suppressing sidelobes in a direction causes an increase in overall white Gaussian noise. In addition, grating lobes cannot be controlled separately from the main lobe.

It is therefore necessary to optimize element positions to avoid grating lobes and large sidelobes within the visible angular region. In an application where the main lobe is steered within a wide angular range, optimization becomes difficult because the angular region from which we have to clear grating lobes widens. Among early works on this topic, King [1] discusses some classes of arrays whose elements are systematically unequally spaced, in logarithmic patterns or patterns based on prime numbers or arithmetic progressions, all in one-dimensional (1D) space.

An array with uniformly spaced elements, at an interval of a half wavelength or less from one another, is one possible solution to the optimization problem, as it does not have grating lobes in the visible angular region. However, because of electromagnetic coupling, this type of array is not suitable for most applications. Therefore, sufficient spacing between each antenna and low sidelobe level with a wide angular coverage must still be simultaneously satisfied.

An array with randomly spaced antenna elements is another possible solution to the optimization problem. Lo [2], Steinberg [3], [4], and Donvito [5] have statistically investigated the sidelobe level of this type of array. Regardless of its simple scheme, this type of array is not practical if the position of elements is unrestricted. One possible approach introduced by Fante [6] to mitigate electromagnetic coupling between elements in a random array is to remove an element when it is closer to another element than a particular threshold. Although this method is effective for an array with a large number of elements, it is not easy to implement unless the is compact in size. In addition, the performance of such an array cannot be regarded as optimum.

An array whose antenna elements are thinned by alternative means is another possible solution of the optimization problem. Holm [7] describes some two-dimensional (2D) array layout optimized with a linear programing algorithm. Murino [8] and Trucco [9] present iterative optimization methods based on certain criteria; their methods are similar to that of this paper except for the evaluation function. Haupt [10], [11] and Bray [12] present genetic algorithms (GAs). Pierro [13] examines some classes of deterministic aperiodic arrangement such as Penrose tiling.

We introduce a simple function to evaluate the beam pattern and propose an algorithm to generate arrays with

low-peak sidelobes within a wide angular range and with sufficient antenna interval [14]. For arrays with a large number of antennas, we also propose a fast algorithm that evaluates antenna spacing. We describe some resulting arrays and show their optimality with certain criteria.

This paper is organized as follows. Section 2 defines a system model based on element positions and beam patterns. Section 3 describes a method for evaluating sidelobe levels, which involves square integration. Section 4 introduces an alternate, faster but equivalent method for evaluating sidelobe levels, which uses the potential function method. Section 5 introduces a simple trial-and-error optimization algorithm to evaluate antenna spacing. Section 6 discusses case studies and the properties of the arrays that result from use of these algorithms. Section 7 presents our conclusions.

2. System Model

In this study, we treat a planar array defined in a two-dimensional space (x, y) that is normalized as

$$\begin{pmatrix} x \\ y \end{pmatrix} = \begin{pmatrix} X/\lambda \\ Y/\lambda \end{pmatrix} \tag{1}$$

where X and Y are physical lengths, and λ is the wavelength. A plane wave observed at normalized antenna position (x, y) that arrives from direction (zenith angle, azimuth) $= (\theta, \phi)$ is described as a complex signal

$$c(\boldsymbol{x}, \boldsymbol{\eta}) = \exp\left(\mathrm{j}2\pi\boldsymbol{\eta} \cdot \boldsymbol{x}\right) \tag{2}$$

where $\boldsymbol{x} = (x, y)^{\mathrm{t}}$ and $\boldsymbol{\eta} = (\sin\theta\sin\phi, \sin\theta\cos\phi)^{\mathrm{t}}$. Note that $\boldsymbol{\eta} = (0, 0)^{\mathrm{t}}$ is the direction perpendicular to the planar array. The visible region of an array from a zenith angle $\theta = 0°$ to $90°$ corresponds to

$$|\boldsymbol{\eta}| \leq 1.$$

Employing the 2D delta function defined by

$$f(\boldsymbol{x}_0) = \int \delta(\boldsymbol{x} - \boldsymbol{x}_0) f(\boldsymbol{x}) \mathrm{d}\boldsymbol{x} \tag{3}$$

where $f(\boldsymbol{x})$ is an arbitrary continuous function, we have an *antenna distribution function*
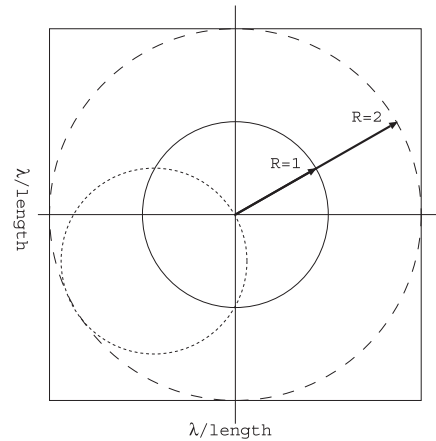
$$a_0(\boldsymbol{x}) = \sum_{n=1}^{N} \delta(\boldsymbol{x} - \boldsymbol{x}_n). \tag{4}$$

where $\boldsymbol{x}_n$ is the position of the n-th antenna. To examine the array response, we define an *antenna function* that describes an array steered to a desired direction $\boldsymbol{\eta}_{\mathrm{d}}$ as

$$a(\boldsymbol{x}) = a(\boldsymbol{x}, \boldsymbol{\eta}_{\mathrm{d}}) = \sum_{n=1}^{N} c^*(\boldsymbol{x}, \boldsymbol{\eta}_{\mathrm{d}}) \delta(\boldsymbol{x} - \boldsymbol{x}_n) \tag{5}$$

where the superscript * denotes a complex conjugate.

The output of the antenna array $a(\boldsymbol{x}, \boldsymbol{\eta}_{\mathrm{d}})$ with incident signal $c(\boldsymbol{x}, \boldsymbol{\eta}_{\mathrm{i}})$, which arrives from a certain direction $\boldsymbol{\eta}_{\mathrm{i}}$, is

Fig. 1 Visible region in $b_0(\boldsymbol{\eta})$ in $\boldsymbol{\eta}$-space. The origin is the main beam; the solid circle is the horizon in $\boldsymbol{x}$-space. The smaller dashed circle is the horizon as it appears when the mainlobe is horizontally tilted. The inside of the larger dashed circle thus corresponds to the entire visible region when all possible mainlobe directions are allowed.

$$s(\boldsymbol{\eta}_d, \boldsymbol{\eta}_{\mathrm{i}}) = \int a(\boldsymbol{x}, \boldsymbol{\eta}_d) c(\boldsymbol{x}, \boldsymbol{\eta}_{\mathrm{i}}) \mathrm{d}\boldsymbol{x} \tag{6}$$

$$= \int \sum_{n=1}^{N} [c^*(\boldsymbol{x}, \boldsymbol{\eta}_{\mathrm{d}}) \delta(\boldsymbol{x} - \boldsymbol{x}_{\mathrm{i}})] c(\boldsymbol{x}, \boldsymbol{\eta}_{\mathrm{i}}) \mathrm{d}\boldsymbol{x} \tag{7}$$

$$= \sum_{n=1}^{N} \exp[\mathrm{j}2\pi(\boldsymbol{\eta}_{\mathrm{i}} - \boldsymbol{\eta}_{\mathrm{d}}) \cdot \boldsymbol{x}]. \tag{8}$$

The output becomes maximum at $s(\boldsymbol{\eta}_{\mathrm{d}}, \boldsymbol{\eta}_{\mathrm{i}}) = N$ for $\boldsymbol{\eta}_{\mathrm{d}} = \boldsymbol{\eta}_{\mathrm{i}}$. If we observe $s(\boldsymbol{\eta}_{\mathrm{d}}, \boldsymbol{\eta}_{\mathrm{i}})$ in (8) as a function of $\boldsymbol{\eta}_{\mathrm{i}}$, the equation can be interpreted as the spatial response of the array, in which case we rewrite the function as $b(\boldsymbol{\eta})$. Therefore, the response $b(\boldsymbol{\eta})$ of the antenna array $a(\boldsymbol{x})$ is defined by a two-dimensional Fourier transform pair:

$$b(\boldsymbol{\eta}) = \int a(\boldsymbol{x}) \exp(\mathrm{j}2\pi\boldsymbol{\eta} \cdot \boldsymbol{x}) \mathrm{d}\boldsymbol{x} \tag{9}$$

$$a(\boldsymbol{x}) = \int b(\boldsymbol{\eta}) \exp(-\mathrm{j}2\pi\boldsymbol{\eta} \cdot \boldsymbol{x}) \mathrm{d}\boldsymbol{\eta}. \tag{10}$$

Hereafter, $b(\boldsymbol{\eta})$ is also referred to as a *beam function*. By these equations, we also have a response $b_0(\boldsymbol{\eta})$ such that

$$a_0(\boldsymbol{x}) \overset{\mathcal{F}}{\Leftrightarrow} b_0(\boldsymbol{\eta}).$$

When the main beam is steered to direction $\boldsymbol{\eta}'$ in (5), the corresponding beam function is

$$b(\boldsymbol{\eta}) = b_0(\boldsymbol{\eta} - \boldsymbol{\eta}'). \tag{11}$$

Then, the visible region for b_0 is given by

$$|\boldsymbol{\eta} - \boldsymbol{\eta}'| \leq 1. \tag{12}$$

If we allow the main beam direction $\boldsymbol{\eta}'$ to steer within $0 \leq \theta \leq \theta_s$, the entire visible region becomes

$$|\boldsymbol{\eta}| \leq 1 + \sin\theta_s. \tag{13}$$

In particular, when $\boldsymbol{\eta}'$ is allowed to steer within all possible directions $0 \leq \theta \leq \pi/2$, the entire visible region for b_0

becomes

$$|\boldsymbol{\eta}| \le 2. \qquad (14)$$

Therefore, grating lobes and sidelobes of $b_0(\boldsymbol{\eta})$ are to be considered within these regions. Figure 1 is the visible region in $\boldsymbol{\eta}$-space. The smaller solid circle ($R = 1$) shows the horizon where the main beam is aimed at the zenith.

3. Method for Evaluating Sidelobe Levels Using Square Integration

The objective of this study is to design arrays that do not have grating lobes and unnecessarily large sidelobes within certain angular regions of interest. We refer to this region as D defined in $\boldsymbol{\eta}$-space. D is defined on an application basis. To evaluate the performance of an array, we introduce a mean-square function in D. Note that this criterion also minimizes the average power of incident noise from a given angular space. Thus, the evaluation function is defined as

$$E = \int_D |b_0(\boldsymbol{\eta})|^2 d\boldsymbol{\eta}. \qquad (15)$$

Using a weight function $\Psi(\boldsymbol{\eta})$ as a integral kernel, the evaluation function is redefined as

$$E = \int |\Psi(\boldsymbol{\eta}) b_0(\boldsymbol{\eta})|^2 d\boldsymbol{\eta} \qquad (16)$$

where

$$\Psi(\boldsymbol{\eta}) = \begin{cases} 1 & (\boldsymbol{\eta} \in D) \\ 0 & \text{otherwise} \end{cases}. \qquad (17)$$

In this study, we define a donut-shaped region as D,

$$D : R_1 \le |\boldsymbol{\eta}| \le R_0. \qquad (18)$$

where R_1 and R_0 are the radii in η-space corresponding to the mainlobe region and the entire visible region, respectively. By setting the weight to 1 within D and to 0 elsewhere, we obtain a donut-shaped weight function $\Psi(\boldsymbol{\eta})$ as shown in Fig. 2. The cavity with radius R_1 is set to exclude the mainlobe from the sidelobe evaluation function. Since R_1 does not sharply affect the output, we set it to the empirical value of 0.1 in the following analyses.

4. Alternate, Faster Method for Evaluating Sidelobe Levels Using the Potential Function Method

To evaluate an array using the evaluation function (16), numerical Fourier transform and numerical integration are required for each time. This time-consuming procedure is not suitable for array optimization, which uses an iterative scheme. In this section, we derive a fast evaluation algorithm that is equivalent to square integration.

The mean-square function for the sidelobe region (16) introduced in the previous section, is restated as

$$E = \int |\Psi(\boldsymbol{\eta}) b_0(\boldsymbol{\eta})|^2 d\boldsymbol{\eta}. \qquad (19)$$
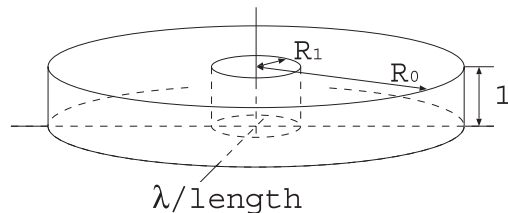

Fig. 2 Weight function $\Psi(\boldsymbol{\eta})$. R_0 and R_1 should be set to the size of visible region and mainlobe region, respectively.
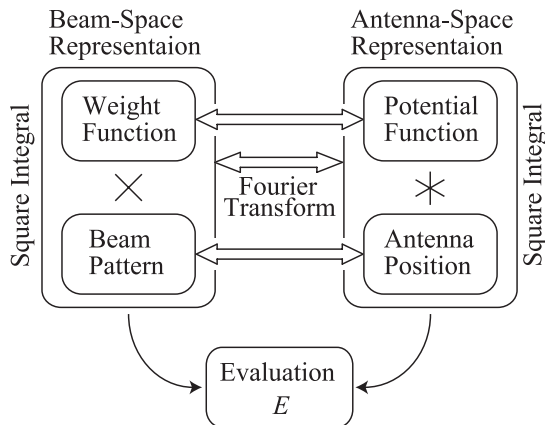

Fig. 3 The relationship between the weight function and the beam patten defined in the beam-space, and the potential function and antenna position defined in the antenna-space. Symbols "×" and "∗" indicate multiplication and convolution, respectively, of two functions. We obtain the same evaluation from the same antenna array with either representation.

According to Parseval's theorem, squared integration in (19) is a preserved quantity for Fourier transform and is written as a function in $\boldsymbol{x}$-space using convolution $*$ as

$$E(\boldsymbol{X}) = \int |(\psi * a_0)(\boldsymbol{x})|^2 d\boldsymbol{x} \qquad (20)$$

$$= \int \left| \sum_{m=1}^{N} \psi(\boldsymbol{x} - \boldsymbol{x}_m) \right|^2 d\boldsymbol{x} \qquad (21)$$

where $\psi(\boldsymbol{x})$ is the 2D Fourier Transform of $\Psi(\boldsymbol{\eta})$:

$$\psi(\boldsymbol{x}) = \frac{R_0 J_1(2\pi R_0 |\boldsymbol{x}|)}{|\boldsymbol{x}|} - \frac{R_1 J_1(2\pi R_1 |\boldsymbol{x}|)}{|\boldsymbol{x}|} \qquad (22)$$

where J_1 is Bessel's function of the first order. We call $\psi(\boldsymbol{x})$ the *potential function* that determines the relative position of elements. Figure 3 shows the relationship between these functions.

This $\psi(\boldsymbol{x})$ is a two-dimensional real function of radial distance, in polar coordinates, around the element shown in Fig. 4. Therefore, the evaluation function calculated at each iteration holds

$$E(\boldsymbol{X}) = \int \left[\sum_{m=1}^{N} \psi(\boldsymbol{x} - \boldsymbol{x}_m) \right]^2 d\boldsymbol{x} \qquad (23)$$

$$= \sum_{n,m=1}^{N} \int \psi(\boldsymbol{x} - \boldsymbol{x}_n) \psi(\boldsymbol{x} - \boldsymbol{x}_m) d\boldsymbol{x}$$
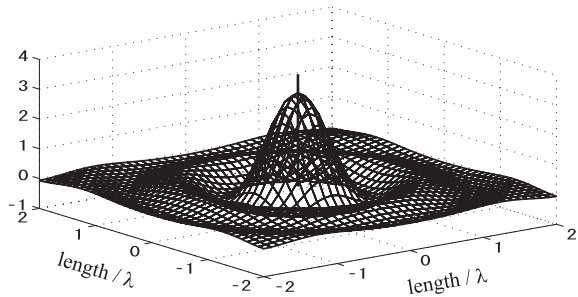
Fig. 4 A potential function $\psi(x)$ in x-space as a Fourier transform of $\Psi(\eta)$ corresponding to $R_0 = 1$.
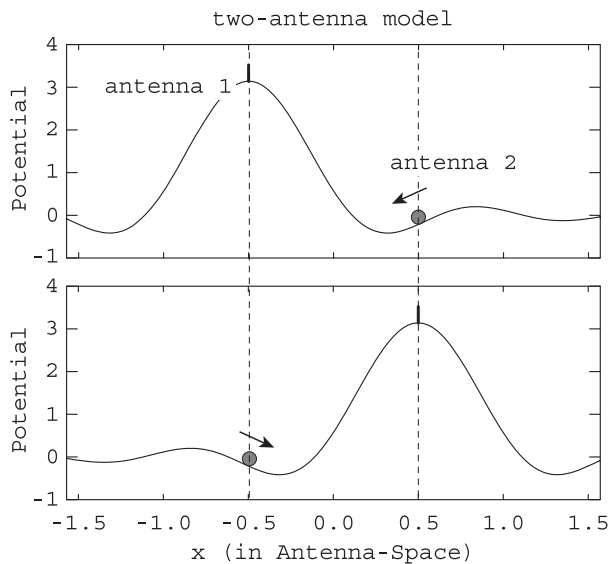

Fig. 5 Schematic illustration of the optimization mechanism in the simplest two-antenna scenario. The X axis is the antenna space with normalized units. The short thick vertical lines and balls on the surface of the potential curves are antennas. The top and bottom panels correspond to the phases in which the positions of antenna 1 and 2 are evaluated.

$$= \sum_{n,m=1}^{N} \int \psi(x)\psi(x + x_n - x_m)\mathrm{d}x. \tag{24}$$

The integration in (24) can be considered as the auto-correlation function of a real function $\psi(x)$. An auto-correlation of a function and the squared absolute of its Fourier transform constitute the following Fourier transform pair:

$$\int \psi(x)\psi(x + x_n - x_m)\mathrm{d}x \overset{\mathcal{F}}{\Leftrightarrow} |\Psi(\eta)|^2 \tag{25}$$

Since the function $\Psi(\eta)$ is defined by (17), the squared absolute is

$$|\Psi(\eta)|^2 = \Psi(\eta). \tag{26}$$

We can thus conclude

$$\int \psi(x)\psi(x + x_n - x_m)\mathrm{d}x = \psi(x_n - x_m). \tag{27}$$

The evaluation function (24) is now restated as

$$E(X) = \sum_{n,m=1}^{N} \psi(x_n - x_m) \tag{28}$$

on condition that

$$\Psi(\eta) = \{0, 1\} \tag{29}$$

where

$$\psi(x) = F[\Psi(\eta)]. \tag{30}$$

Equation (28) has neither Fourier transform nor integration, and so can be calculated much faster than the original expression, but provides the identical result. Based on (28), the minimization algorithm can be made much faster by means of the steepest descent method. Figure 5 schematically illustrates the concept based on a two-antenna model.

5. A Trial-and-Error Optimization Algorithm

We introduce a simple trial-and-error array optimization algorithm using the evaluation scheme discussed in the previous section to show how the mean-square evaluation function works. In this section, we use the collective notation X to represent a set of antenna positions $(x_1, \cdots, x_n)$ with which an antenna distribution function can conveniently be written as

$$a_0(X) = \sum_{i=1}^{n} \delta(x - x_i). \tag{31}$$

This algorithm consists mainly of perturbations, evaluations, and updates. At each iteration, the algorithm first suggests a temporary position X such that $X^{(\mathrm{temp})} = X^{(i-1)} + \Delta X$ where $X^{(i-1)}$ is the antenna position determined at the previous step and ΔX is a small random perturbation. Second, the algorithm calculates the evaluation $E^{(\mathrm{temp})}$ is calculated by (28) in terms of the temporary distribution $a_0(X^{(\mathrm{temp})})$. Third, the algorithm adopts a candidate set of positions $X^{(\mathrm{temp})}$ as $X^{(i)}$ if $E^{(\mathrm{temp})}$ is better than the previous $E^{(i-1)}$, or discard it otherwise. In these processes, the standard deviation of ΔX is diminished if no update is made during a couple of iterations. These processes are repeated until the evaluation E is assumed to be minimized.

In a real implementation, the series of processes from perturbation to update/discard should be made for each element separately to reduce the probability of discard for a better convergence. The steps of this algorithm are as follows:

Initialization part: (Do only the first time)

  1 Set the initial position to $X^{(0)} = \mathbf{0}$.

  2 Calculate the initial evaluation by (28).

Iteration part:

for ith iteration

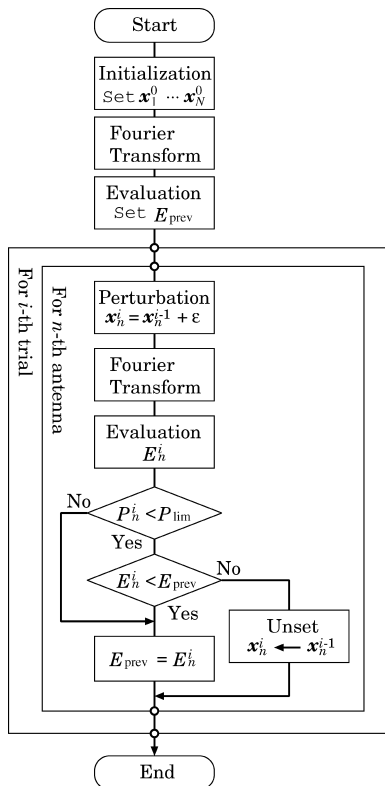**Fig. 6** A flow chart summarizing the trial-and-error algorithm.

Fig. 7 Convergence of the evaluation over iteration for 12-antenna arrays with 3-fold symmetry. The arrangement of an array is almost optimized and fixed in 50 times of evaluation.

for nth element

1 Impose random perturbation Δx_n on top of the previous position such that $x_n^{(\text{temp})} = x_n^{(i-1)} + \Delta x_n$.

2 Calculate the evaluation by (28).

3 Set or discard the temporary position according to $E^{(\text{temp})}$.

$$\begin{cases} x_n^{(i)} = x_n^{(\text{temp})} & (\text{when } E^{(\text{temp})} < E^{(\text{prev})}) \\ x_n^{(i)} = x_n^{(i-1)} & (\text{otherwise}). \end{cases}$$

 end for

 end for

Figure 6 shows the algorithm flow. Figure 7 shows the convergence property obtained for the case of a 120° rotational symmetric 12-element array that is discussed in Sect. 6. Since the optimization is performed using random perturbation to evolve the array geometry, the resulting arrangement differs every time. Properties of the resulting array are discussed later.

For evaluating the position of antenna 2, the potential function formed only by the other antenna is assumed, and vice versa. In this case, antennas 1 and 2 descend the potential curves. Finally, the two antennas (and the potentials simultaneously) approach each other and stop when they find the minimal points of the potentials.
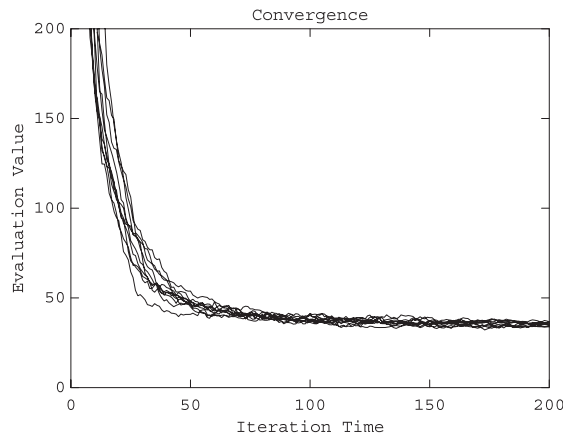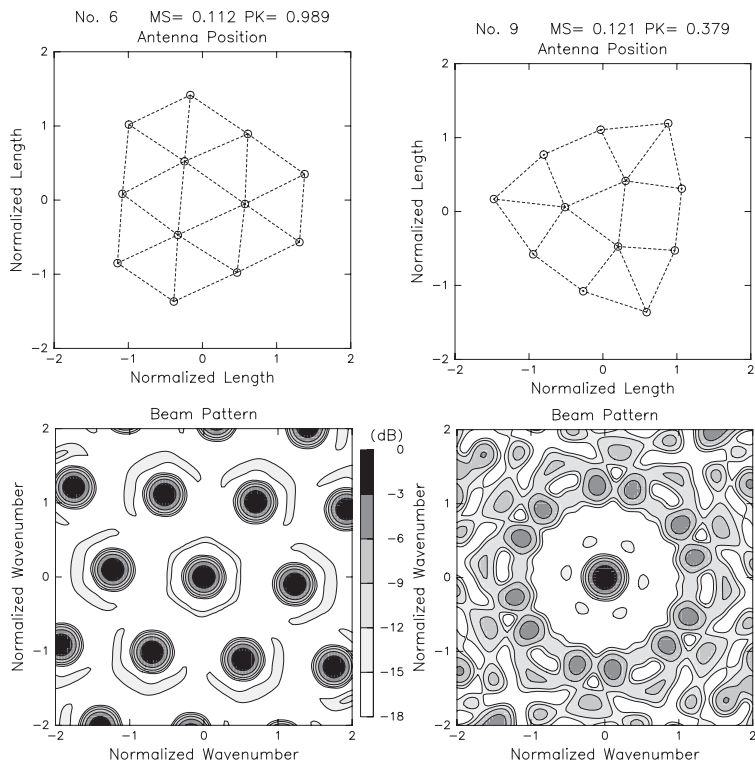
6. Resulting Arrays

First, we show the basic behavior of our evaluation scheme and algorithm with simple models. We discuss 12-element arrays under the constraint of 3-fold rotational symmetry, which has the degrees of freedom of 4 elements. In the initial state, all elements are at the origin. To realize a 3-fold symmetric 12-element array, only 4 elements are taken into account and are tripled at every 120° around the origin before evaluation.

Let N denote the number of elements. We conducted 10,000 separate optimizations for the case $N = 12$. Figure 8 (left) shows the most frequent result. This type of array has a minimum mean-square response that corresponds to the global minimum of the optimization problem. However, equilateral-triangular-type arrays have grating lobes and are not suitable for wide-scanning array applications.

Figure 8 (right) shows the next most frequent result. This solution should be at a local minimum of the problem. This triangular-rectangular-type array yields much a better beam pattern than does the equilateral-triangular-type array. It does not have grating lobes within the visible region and has sufficiently low sidelobes around the mainlobe.

To compare these arrays, we introduce the following quantitative evaluations: peak sidelobe, minimum distance between antennas, and mean-square sidelobe. Figure 9 shows a scattering diagram of the peak and mean-square sidelobe response of each result. The equilateral-triangular-type array distributes its peak/mean-square points around the top-left corner of the diagram. The top of the Y axis (peak sidelobe = 1.0) correponds to grating lobe, which is the same level as main lobe. The bottom-left corner is the best point in terms of both peak and mean-square evaluation. Based on this criterion, the triangular-rectangular-type array shows superior performance.

Figure 10 shows a scattering diagram of peak vs. minimum distance between antennas. Sufficient clearance between antennas is important for a real implementation, to

Fig. 8 Resulting arrays generated by the trial-and-error algorithm under the constraint of 3-fold rotational symmetry. (Left) A typical triangular array that most frequently appears corresponding to the global minimum of the square integration. (Right) Another typical array that arises at a local minimum of the evaluation.
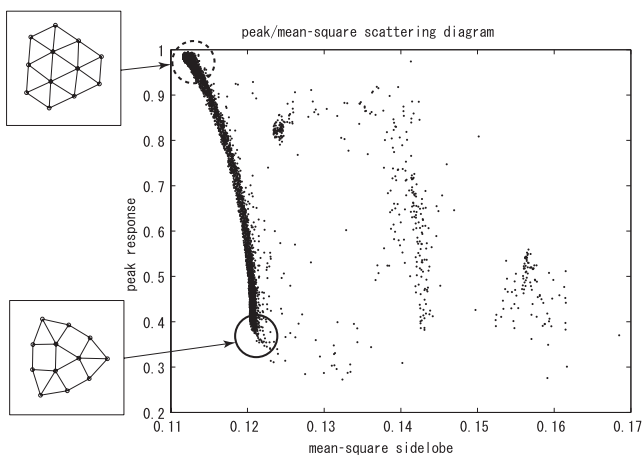
Fig. 9 The scattering diagram for the peaks vs. mean-square sidelobe responses of 10,000 arrays generated by the proposed algorithm.
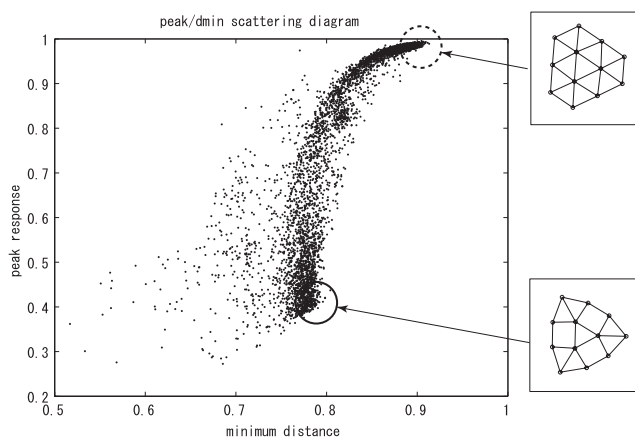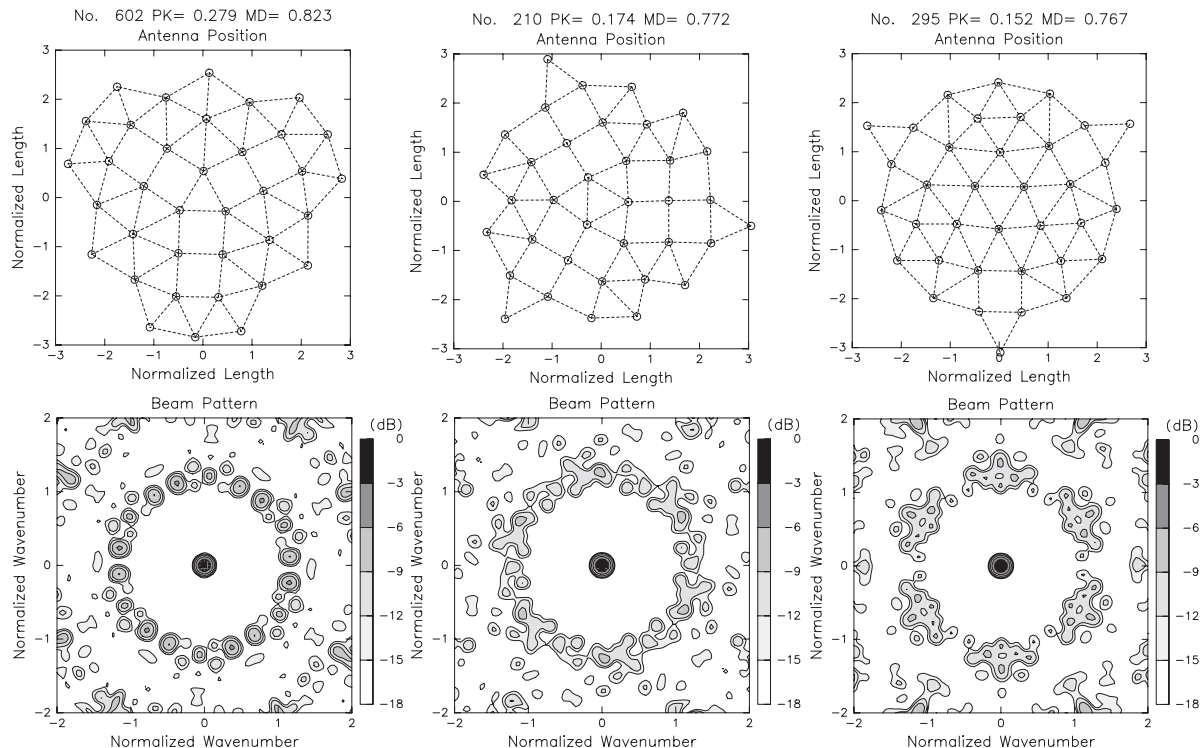

Fig. 10 Same as Fig. 9 but for the peaks vs. the minimum distance of each antenna.

avoid degradation of performance because of undesired electromagnetic coupling. Based on this criterion, the triangular-rectangular-type array also shows superior performance.

We also tried separate 10,000 optimizations for the case $N = 36$ with 3-fold symmetric constraint. R_0 and R_1 are set to 1.0 and 0.1, respectively. Figure 11 shows three selected results. Figure 12 shows plots of peaks and minimum distances. The points in Fig. 12 scatter in a more complex form

than those in Fig. 10, due to the larger degrees of freedom. Although, in the diagram, arrays plotted at the bottom-right corner are preferable, the corner cannot be uniquely identified. The array at the left panel of Fig. 11 has the largest peak sidelobe (0.279) and largest minimum distance (0.823) within the three examples. The array at the right panel has the smallest peak sidelobe of 0.152 (-8.18 dB) and smallest minimum distance (0.767) of the three. The results show effective tradeoffs between the two evaluation factors.

No. 602 PK= 0.279 MD= 0.823
Antenna Position

No. 210 PK= 0.174 MD= 0.772
Antenna Position

No. 295 PK= 0.152 MD= 0.767
Antenna Position

Beam Pattern

Beam Pattern

Beam Pattern

Fig. 11 Resulting arrays of a case $N = 36$ with the 3-fold symmetric constraint. At the top of each panel, the peak sidelobe ("PK") and the minimum distance between antennas ("MD") are shown.

peak/dmin scattering diagram
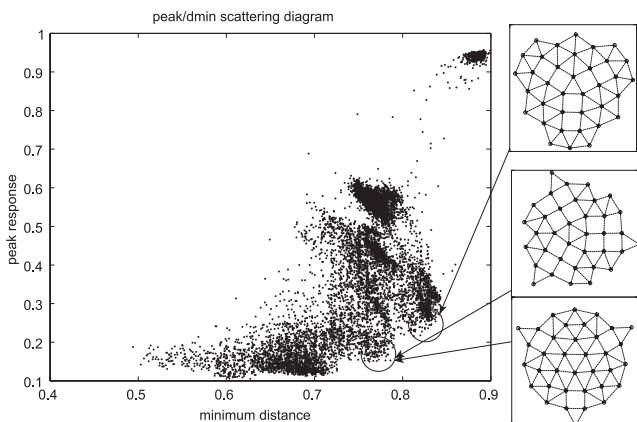
Fig. 12 The scattering diagram of the peaks vs. minimum distance for 10,000 arrays with $N = 36$ under the constraint of 3-fold symmetry.

7. Conclusions

The potential function method, which effectively describes the relationship between the weighting function for spatial response and element positions, is useful for evaluating an array multiple times. Although square integration itself does not perfectly evaluate an array, the proposed algorithm generates good results as it falls to a local minimum. Some of the arrays, thus, make effective tradeoffs between low-peak sidelobes and large element-to-element separations. Those arrays that placed on the edge of the scatter diagrams of

these evaluation factors form sets of optimal arrays in this respect although, in principle, it is impossible to select only one of them as optimum without specifying its application. For large-array applications, in the future, a more systematic algorithm is needed to avoid time-consuming multiple runs.

References

[1] D.D. King, R.F. Packard, and R.K. Thomas, "Unequally-spaced, broad-band antenna arrays," IRE Trans. Antennas Propag., pp.380–384, July 1960.

[2] Y.T. Lo, "A mathematical theory of antenna arrays with randomly spaced elements," IEEE Trans. Antennas Propag., pp.257–268, May 1964.

[3] B.D. Steinberg, "The peak sidelobe of the phased array having randomly located elements," IEEE Trans. Antennas Propag., vol.AP-20, no.2, pp.129–136, March 1972.

[4] B.D. Steinberg and E.H. Attia, "Sidelobe reduction of random arrays by element position and frequency diversity," IEEE Trans. Antennas Propag., vol.AP-31, no.6, pp.922–930, 1983.

[5] M.B. Donvito and S.A. Kassam, "Characterization of the random array peak sidelobe," IEEE Trans. Antennas Propag., vol.AP-27, no.3, pp.379–385, May 1979.

[6] R.L. Fante, G.A. Robertshaw, and S. Zamoscianyk, "Observation and explanation of an unusual feature of random arrays with a nearest-neighbor constraint," IEEE Trans. Antennas Propag., vol.39, no.7, pp.1047–1049, 1991.

[7] S. Holm, B. Elgetum, and G. Dahl, "Properties of the beampattern of weight- and layout-optimized sparse arrays," IEEE Trans. Ultrason. Ferroelectr. Freq. Control, vol.44, no.5, pp.983–991, Sept. 1997.

[8] V. Murino, A. Trucco, and C.S. Regazzoni, "Synthesis of unequally spaced arrays by simulated annealing," IEEE Trans. Signal Process., vol.44, no.1, pp.119–123, Jan. 1996.

[9] A. Trucco, "Thinning and weighting of large planar arrays by simulated annealing," IEEE Trans. Ultrason. Ferroelectr. Freq. Control, vol.46, no.2, pp.347–355, March 1999.

[10] R.L. Haupt, "Thinned arrays using genetic algorithms," IEEE Trans. Antennas Propag., vol.42, no.7, pp.993–999, July 1994.

[11] R.L. Haupt, "Interleaved thinned linear arrays," IEEE Trans Antennas Propag., vol.53, no.9, Sept. 2005.

[12] M.G. Bray, D.H. Werner, D.W. Boeringer, and D.W. Machuga, "Optimization of thinned aperiodic linear phased arrays using genetic algorithms to reduce grating lobes during scanning," IEEE Trans. Antennas Propag., vol.50, no.12, pp.1732–1742, Dec. 2002.

[13] V. Pierro, V. Galdi, G. Castaldi, I.M. Pinto, and L.B. Felsen, "Radiation properties of planar antenna arrays based on certain categories of aperiodic tilings," IEEE Trans. Antennas Propag., vol.53, no.2, pp.635–644, Feb. 2005.

[14] K. Nishimura and T. Sato, "A fast optimization method of two-dimensional antenna array for adaptive beamforming," Proc. IEEE AP-S Symp., pp.3395–3398, 2006.

Koji Nishimura was born in Kyoto, 1975. He received the B.E. degree from Ritsumeikan University, Japan, in 1999, and the M.I. and Ph.D. degrees from Kyoto University, Japan, in 2001 and 2006, respectively. From 2001 to 2003, he was with Sony Corporation. Currently, he is a postdoctral researcher at Transdisciplinary Research Integration Center, Research Organization of Information and Systems, Japan. Dr. Nishimura received the Best Paper Award in the Eleventh International Workshop on Technical and Scientific Aspects of MST Radar in 2006. He is a member the IEEE.

Toru Sato received his B.E., M.E., and Ph.D. degrees in electrical engineering from Kyoto University, Japan, in 1976, 1978, and 1982, respectively. He has been with Kyoto University since 1983 and is currently a professor in the Graduate School of Informatics. His major research interests have been system design and signal processing aspects of atmospheric radars, radar remote sensing of the atmosphere, observations of precipitation using radar and stellite signals, radar observation of space debris, and signal processing for subsurface radar signals. Dr. Sato was awarded the Tanakadate Prize in 1986. He is a member of the IEEE. the Society of Geomagnetism and Earth, Planetary and Space Science, the Japan Society for Aeronautical and Space Sciences, and the Americal Meteorological Society.